AIP | Applied Physics Letters

Controlling the carrier lifetime of nearly threading-dislocation-free ZnO homoepitaxial films by 3d transition-metal doping

S. F. Chichibu, K. Kojima, Y. Yamazaki, K. Furusawa, and A. Uedono

Citation: Applied Physics Letters **108**, 021904 (2016); doi: 10.1063/1.4939838
View online: http://dx.doi.org/10.1063/1.4939838
View Table of Contents: http://scitation.aip.org/content/aip/journal/apl/108/2?ver=pdfcov
Published by the AIP Publishing

Controlling the carrier lifetime of nearly threading-dislocation-free ZnO homoepitaxial films by 3*d* transition-metal doping

S. F. Chichibu,[1,a)] K. Kojima,[1] Y. Yamazaki,[1] K. Furusawa,[1] and A. Uedono[2]
[1]*Institute of Multidisciplinary Research for Advanced Materials, Tohoku University, 2-1-1 Katahira, Aoba, Sendai 980-8577, Japan*
[2]*Division of Applied Physics, Faculty of Pure and Applied Sciences, University of Tsukuba, Tsukuba, Ibaraki 305-8573, Japan*

(Received 23 November 2015; accepted 31 December 2015; published online 13 January 2016)

Carrier lifetime in nearly threading-dislocation-free ZnO homoepitaxial films was controlled by doping 3*d* transition-metals (TMs), Ni and Mn. The photoluminescence lifetime of the near-band-edge emission (τ_{PL}) was decreased linearly by increasing TM concentration, indicating that such TMs are predominant nonradiative recombination centers (NRCs). From this relationship, exciton capture-cross-section (σ_{ex}) of 2.4×10^{-15} cm^2 is obtained. Because σ_{ex} of native-NRCs (Zn-vacancy complexes) is likely larger than this value, the linear dependence of the internal quantum efficiency on τ_{PL} observed in our TM-doped ZnO and unintentionally doped ZnO in literatures indicates that the concentrations of native-NRCs in the latter are "lower than" 10^{16}–10^{17} cm^{-3}.
 [http://dx.doi.org/10.1063/1.4939838]

Wide bandgap (E_g) wurtzite ZnO and related $Mg_xZn_{1-x}O$ alloys[1] are an excellent candidate for the use in visible[2,3] and ultraviolet (UV)[4] light-emitting diodes (LEDs), because of attractive material properties of ZnO such as large E_g of 3.36 eV at 300 K (Ref. 5) and large exciton binding energy of 59 meV.[6] Although white LEDs[7] composed of an InGaN quantum well LED[8] and yellow-light-emitting phosphors have been distributed world-wide,[9] there still remain significant problems such as low color-rendering-index due to their complimentary white color and sleep disturbance due to strong blue lights. For solving these problems, fabrication of true white LEDs composed of a near UV LED and red, green, and blue light-emitting phosphors at low cost is an ultimate solution. To comply with this demand, ZnO-based LEDs are attractive because the low threading-dislocation (TD) density, large-size, and highly pure ZnO homoepitaxial substrates can be grown at low cost using the hydrothermal (HT) technique.[10] In addition, ZnO and $Mg_xZn_{1-x}O$/ZnO heterostructure are possible candidates for realizing radiation-resistant thin-film-transistors[11] and heterostructure field-effect-transistors,[12] as quantum Hall effects have been demonstrated at the $Mg_xZn_{1-x}O$/ZnO heterointerface at low temperature.[13]

For designing advanced optical and electronic devices using ZnO, in-depth probing and control of the free-carrier lifetime ($\tau_{carrier}$) in the constituent layers are essential. Especially, controlling the minority carrier lifetime ($\tau_{minority}$) is indispensable, because it reflects the recombination lifetime and determines the diffusion length, and eventually determines the device performances. In the case of direct bandgap semiconductors such as ZnO, $\tau_{minority}$ can be simply measured by using time-resolved photoluminescence (TRPL) measurement under low-excitation conditions. The photoluminescence (PL) lifetime (τ_{PL}) of the near-band-edge (NBE) emission is equal to $\tau_{minority}$ and is expressed as

$$\tau_{PL}^{-1} = \tau_R^{-1} + \tau_{NR}^{-1}, \tag{1}$$

where τ_R and τ_{NR} are radiative and nonradiative recombination lifetimes, respectively. Here, τ_R is inverse of the radiative recombination rate (R_R) and reflects the intrinsic radiative performance of the material. Thus, τ_R is a unique value to the material without quantum confinements. On the other hand, τ_{NR} is inverse of the nonradiative recombination rate (R_{NR}) and thus inversely proportional to the concentration of nonradiative recombination centers (NRCs), [NRC]. These parameters are quite important, since they determine the internal quantum efficiency (η_{int}) of the NBE emission under the relation

$$\eta_{int} = R_R/(R_R + R_{NR}) = (1 + \tau_R/\tau_{NR})^{-1}. \tag{2}$$

Accordingly, long τ_{NR} is preferred for optical devices such as LEDs, laser diodes, and solar cells. Long τ_{NR} is also required for low on-resistance and high-voltage-resistant power devices, because Shockley-Read-Hall (SRH)-type midgap NRCs are the cause of recombination and generation currents and eventually lower the breakdown voltage. Hence, [NRC] should be minimized in these devices. Excessively long $\tau_{carrier}$, on the other hand, will result in considerably long recovery time, leading to limited switching frequency and considerable switching loss.

As the first step to control $\tau_{minority}$, one must know the exact origin of the lifetime killer to use. Because the doping of midgap radiative recombination centers causes unnecessary photon population, doping NRCs is typically used. In the case of single crystalline epilayers of ZnO, the authors have first clarified that point-defect complexes incorporated with Zn-vacancies (V_{Zn}) such as $V_{Zn}X$, where X is unidentified yet but likely O-vacancies (V_O), are the

[a)]Author to whom correspondence should be addressed. Electronic mail: chichibulab@yahoo.co.jp

predominant "native-" SRH-type NRCs, from the results of room-temperature TRPL and positron annihilation spectroscopy (PAS) measurements.[14,15] This assignment is complementary, as the origin of NRCs in GaN, which has comparably small lattice parameters and large E_g, has been attributed to point-defect complexes containing Ga-vacancies,[16] by using the same methods. Although τ_{NR} of the ZnO epilayers has been found to depend on the growth temperature (T_g), cooling rate (R_c), and oxygen partial pressure during the cooling (P_{O_2}),[14,15] it cannot be controlled independently of those conditions. Then, controlled doping of SRH-type NRCs allows one to design τ_{NR}. For this purpose, 3*d* transition-metals (TMs) are an excellent candidate, as several of isoelectronic TMs such as Mn,[17] Co,[17,18] and Ni[17,18] have been reported to form 2+/3+ charge transfer levels (CTLs) in the lower half of E_g of ZnO, while Fe[17,19] and Cr[17] do in the upper half. The former three tend to act as deep electron traps and the latter as shallower deep donors in natural n-type ZnO, and both of them can act as NRCs when the material is excited and TMs become empty state. The TMs are known to pin the Fermi level (E_F) on their CTL to obtain semi-insulating property, and also known to become a constituent element of dilute magnetic semiconductors alloyed with ZnO.[20]

In this letter, the results of steady-state PL and TRPL measurements on TM-doped ZnO epilayers are shown to correlate the room-temperature τ_{PL} and quenching ratio (R_q) of the NBE emission with the TM concentration ([TM]), where R_q is defined as the ratio of the integrated spectral intensity at a given temperature to that at low temperature (10 K) and approximates η_{int}. We chose Ni and Mn as TM dopants, and homoepitaxial films were grown on a nearly TD-free HT-ZnO substrate[10] to eliminate possible interferences by TDs. The τ_{PL} value is shown to decrease linearly by increasing [TM], indicating that the TMs are the predominant NRCs. The exciton capture-cross-section (σ_{ex}) is estimated to be 2.4×10^{-15}cm^2. From the linear dependence of R_q on τ_{PL} found universally in the epilayers containing native-NRCs[15,21–23] and TMs, the concentrations of native-NRCs ([V_{Zn}X]) in unintentionally doped (UID) ZnO in literatures[2–4,14,15,21–23] are estimated to be "lower than" 10^{16}–10^{17} cm^{-3}.

Approximately 300 to 1400-nm-thick, (0001) Zn-polar TM-doped ZnO epilayers[24] were grown by the helicon-wave-excited-plasma sputtering epitaxy (HWPSE) method[25] by sputtering a 50-mm-diam. polycrystalline or (0001) Zn-polar crystalline ZnO target on a 500-μm-thick (0001) Zn-polar ZnO substrate. We used this method, because it can grow nearly TD-free ($<10^5$ cm^{-2}) ZnO epitaxial films exhibiting atomically smooth surface morphology with 0.25-nm-high monolayer atomic step lines,[24,26] and thus any possible interferences by TDs can be eliminated. As a matter of fact, all the samples exhibited well-aligned monolayer atomic step lines and TD density was less than 10^5 cm^{-2}.[24] The polycrystalline target was grown by the chemical vapor transport (CVT) technique (Eagle Picher),[27] while the substrate and the crystalline target were grown by HT technique (Tokyo Denpa).[10] The Li impurities originating from the mineralizer used in the HT process were out-diffused from their surfaces using high temperature annealing. The substrate was pretreated following the procedure described in Ref. 28 so that any residual colloidal silica particles can be eliminated. The TM-doping was carried out by placing a tiny Ni-based metal containing Mn impurity adjacent to the substrate. We chose Ni and Mn as the dopants, because both of them have been reported to form 2+/3+ CTLs approximately 1 eV above the valence band (E_V) top of ZnO, namely, $E_V + 0.6 \sim 1.2$ eV for $Ni^{2+/3+}$ and $E_V + 0.9$ eV for $Mn^{2+/3+}$.[17] For exciting the helicon-wave-excited-plasma, a mixture of electronic-grade Ar and O_2 gases was introduced in a remote quartz tube, where a weak magnetic field gradient (~0.01 T) was applied. The fraction of O_2 gas flow rate in the total one was varied between 0.3 and 0.4. The background and growth pressures were 2×10^{-5} and 7×10^{-2} Pa, respectively. The radio-frequency power was varied from 200 to 320 W, while the target bias was controlled (~350 V) to achieve a constant growth rate of ~150 nm/h. After growing the epilayers at high T_g between 950 and 970 °C, they were gradually cooled with $R_c = -10$ °C/min, in order to decrease [V_{Zn}X].[14,15]

The atomic concentrations of TMs (Ni, Mn, and Fe) and residual Al, B, C, Cr, Li, and Si were quantified by secondary-ion-mass spectrometry (SIMS). The concentrations of B, C, Cr, Li, and Si were lower than the detection limits, and the PL peaks peculiar to B, Ga, and In shallow donors[29,30] were not detected.[24] The concentrations of Ni and Mn and residual Fe and Al are summarized in Table I. The sample identification (ID) numbers N1 ~ N6 are given following the order of increasing [TM] being 3×10^{17} to 4×10^{18} cm^{-3}.

Monoenergetic PAS measurement[31,32] was carried out using the positron beam line[32] to inspect the concentration of point defects. Two characteristic parameters are usually used to evaluate a semiconductor.[14,15,31,32] One is the *S* parameter, which in general reflects the concentration (or size) of positron (e^+) trapping centers. In UID-ZnO, negatively charged vacancy-type point defects such as V_{Zn} and V_{Zn}X fall under this category. However, because *S* of Mn- (or MnO_2)-doped ZnO[33] and NiO-doped Al_2O_3[34] have been reported to be larger than that of pure ZnO and Al_2O_3 matrices due to the e^+ annihilation in the vicinity of Mn in ZnO and NiO in Al_2O_3, we concentrate on another parameter, the positron diffusion length (L_+), in this study. The L_+ can be used as a measure of inverse third root of gross concentration of e^+ trapping centers and scattering centers in three-dimensional space, because both centers shorten L_+. The scattering centers are positively charged and neutral point defects such as V_O, interstitials (Zn_i and O_i), and certain complexes.[32] The L_+ values obtained for the present samples were in the range of 35–62 nm. We note that L_+ values for N1 and N2 were 53 and 62 nm, respectively, which are longer than that of the bulk ZnO single crystal grown by the CVT method.[15] Precise control of the growth stoichiometry[26] keeping the step-flow growth mode[24,26] at high T_g[14,15] must be the reason why those record-long L_+ values were obtained. These long[32] L_+ indicate that V_{Zn} concentration ([V_{Zn}]), which directly connects to "native" [NRC], and V_O concentration ([V_O]) were sufficiently low to observe τ_{PL} longer than 400 ps at 300 K.[14,15]

Steady-state PL was measured by using the 325.0 nm line of a cw He-Cd laser (38 W/cm^2) and a spectrometer (*f*/4) with a charge-coupled device camera. In TRPL measurement, a

TABLE I. Comparison of room-temperature values of R_q and τ_{PL} for the NBE emission of TM-doped Zn-polar ZnO epilayers.

Sample identification (ID) number	Concentration (cm^{-3})				R_q (%)	τ_{PL} (ps)
	Ni	Mn	Fe	Al		
N1	3×10^{17}	N.A.	4×10^{16}	2×10^{16}	0.63	65
N2	5×10^{17}	N.A.	1×10^{17}	4×10^{16}	0.24	25
N3	2×10^{17}	4×10^{17}	1×10^{17}	2×10^{16}	0.32	23
N4	4×10^{17}	4×10^{17}	1×10^{17}	2×10^{16}	0.14	26
N5	8×10^{17}	7×10^{16}	N.A.	1×10^{17}	0.11	20
N6	2×10^{18}	2×10^{18}	N.A.	1×10^{18}	0.10	18

frequency-tripled beam of a mode-locked Al_2O_3:Ti laser (266 nm, 120 nJ/cm^2 per pulse) was used for excitation. Temporal emission dynamics were captured using the same type of the spectrometer but equipped with a streak-camera with temporal resolution of 8 ps. We note that, for both measurements, weak excitation conditions were maintained to underline the nonradiative recombination processes. For example, excited electron-hole (e–h) pair concentration for the PL measurement is estimated to be 1.2×10^{15} cm^{-3} when the average τ_{PL} is 50 ps.

The NBE PL spectra of the representative ZnO epilayer (N1) are shown as a function of temperature (T) in Fig. 1(a). The low-temperature spectra were dominated by energetically narrow luminescence peaks originating from the recombinations of A- and B-free excitons (FX_A and FX_B, respectively), those bound to a neutral Al donor ($I_{Al,A}$ and $I_{Al,B}$), and their LO phonon replicas.[24] Detailed discussion of the low-temperature PL spectra have been given in Ref. 24. With increasing T, FX_A peak (at around 3.3 eV at 300 K) took over the spectrum. Although the data are not shown here, the intensity of the PL bands ranging between 2.2 and 2.4 eV was approximately 3 orders of magnitude lower than that of the FX_A peak, implying that the concentration of corresponding point defects (V_O or Zn_i)[35] is lower than or comparable to that of the substrate.[24] Figure 1(b) displays Arrhenius plot of R_q for the whole NBE emission. Different from the cases of UID-ZnO epilayers[15,21] that do not contain TMs, R_q started to decrease even at low temperatures, meaning that photoexcited carriers, or more precisely excitons, are trapped by NRCs immediately after they gain finite diffusion coefficient. Consequently, R_q at 300 K was only 0.63% for this particular sample. The R_q value tended to decrease with increasing [TM], as summarized in Table I.

A representative set of TRPL signals extracted from FX_A components of N1 are shown as a function of T in Fig. 2(a). The decay curves above 30 K can be fitted using a single exponential function. The τ_{PL} value did not show a remarkable change from 10 to 300 K, being 65 ps at 300 K. Because R_q started to decrease at around 20 K and was as low as 0.63% at 300 K, as shown in Fig. 1(b), the observed τ_{PL} is almost equal to τ_{NR}. This τ_{NR} (65 ps) is far shorter than what is expected for an n-type ZnO exhibiting $L_+ = 53$ nm, because τ_{PL} at 300 K of such a ZnO of low [V_{Zn}X] would be 1–2 ns.[14,15] This result indicates that TMs act as predominant NRCs. Room-temperature temporal responses of the FX_A emission of all the epilayers are compared in Fig. 2(b). The τ_{PL} values are seen to decrease with increasing [TM], as summarized in Table I, and all values are smaller than that of the representative value for a HT-ZnO substrate being about 300 ps, as shown in the inset.

The room-temperature τ_{PL} values are plotted as a function of [TM] (Ni and Mn concentration) in Fig. 3. The τ_{PL}

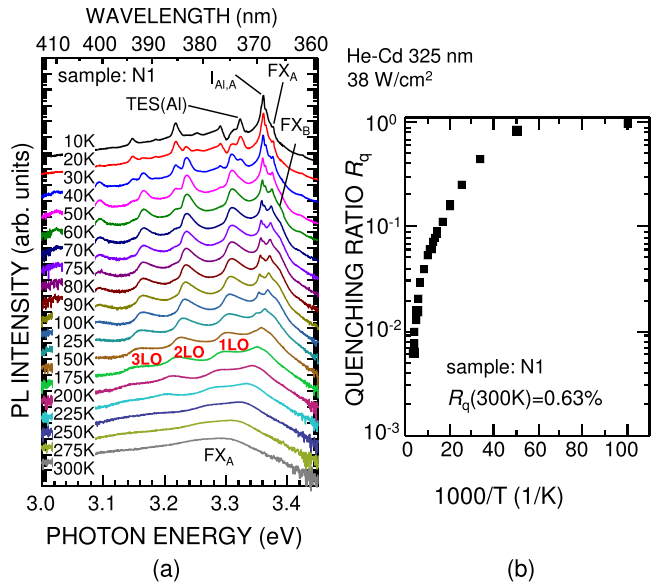

FIG. 1. (a) Representative temperature dependency of the NBE-PL spectra and (b) Arrhenius plot of integrated NBE-PL intensity of nearly TD-free TM-doped ZnO epilayer (N1).

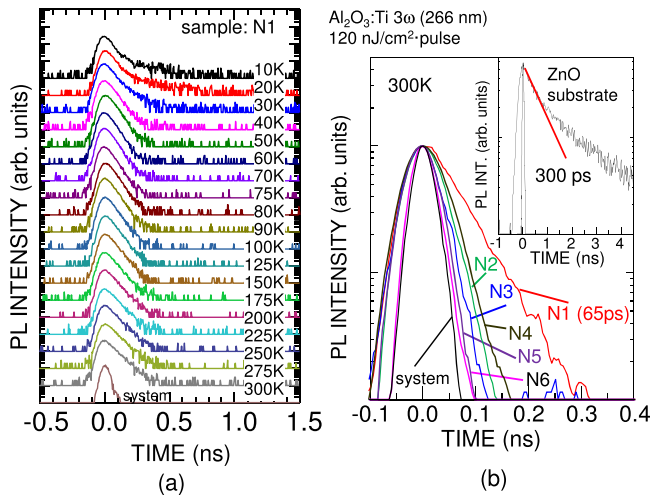

FIG. 2. (a) Examples of temporal decay signals for the FX_A peak of the TM-doped ZnO (N1) at different temperatures and (b) room-temperature signals of all the samples. The inset shows the signal of typical HT-ZnO substrate, of which τ_{PL} of the fast component was about 300 ps.

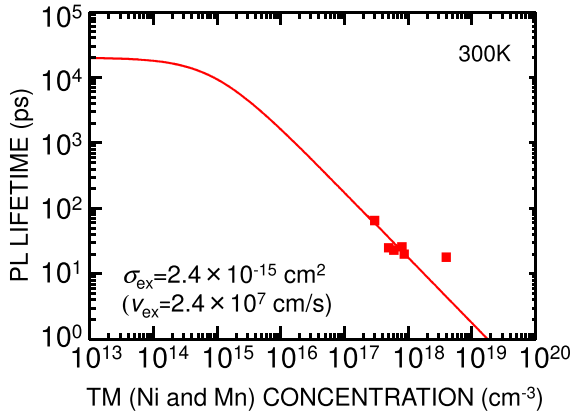

FIG. 3. Room-temperature τ_{PL} values of the FX_A peak in TM-doped ZnO epilayers as a function of gross concentration of TMs ([TM]), namely, Ni and Mn. Solid line shows the fitted τ_{PL}-[TM] relation using Eq. (4), where the values of $\tau_R = 20$ ns (Ref. 15) and $m^*_{ex} = 0.242m_0$[36] were used.

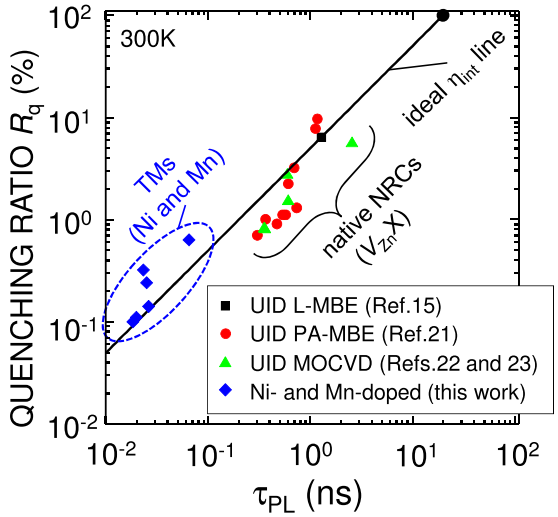

FIG. 4. Room-temperature R_q values of FX_A peak in the TM-doped ZnO epilayers as a function of τ_{PL} (diamonds). Solid line shows ideal $\eta_{int} - \tau_{PL}$ line drawn using the relation $\eta_{int} = \tau_{PL}/\tau_R$, assuming the intrinsic τ_R of 20 ns.[15] For comparison, $R_q - \tau_{PL}$ relations reported for UID ZnO epilayers[15,21–23] are plotted (square, circles, and triangles). The major NRCs in those samples[15,21–23] are "the native" one, $V_{Zn}X$.[14,15]

value was decreased nearly linearly by increasing [TM], confirming that Ni and Mn act as the major NRCs, and [$V_{Zn}X$] is lower than [TM]. Because all the samples showed intermediate to highly resistive n-type conductivity, holes are the minority carriers. This is consistent with the facts that Al concentration was about 10^{16} to 10^{18} and excited *e–h* pair concentration was about 1.2×10^{15} cm^{-3}. Because excited holes in ZnO immediately form excitons, σ_{ex} of the TMs shall be derived from τ_{PL}-[TM] relation, as follows. We assume all Ni and Mn atoms are either in the stable Ni^{2+} (Mn^{2+}) or unstable Ni^{3+} (Mn^{3+}) states in ZnO;[17] [TM] = [TM^{2+}] + [TM^{3+}]. In n-type ZnO, the majority of Ni (Mn) ions are in the neutral Ni^{2+} (Mn^{2+}) state. During the PL process, [Ni^{3+}] and [Mn^{3+}] change with time because of the photoexcited electron and/or exciton trapping. Because of low excitation conditions, [Ni^{3+}] and [Mn^{3+}] are much lower than [Ni^{2+}] and [Mn^{2+}]. Then, $\tau_{minority} = \tau_{NR}$ can be simply expressed by

$$\tau_{NR}^{-1} = v_{ex}\sigma_{ex}[TM], \tag{3}$$

where v_{ex} and σ_{ex}, respectively, denote the thermal velocity $\sqrt{3kT/m^*_{ex}}$ and exciton capture-cross-section. Here, m^*_{ex} is a reduced exciton effective mass. Combining Eqs. (1) and (3), we obtain

$$\tau_{PL}^{-1} = \tau_R^{-1} + v_{ex}\sigma_{ex}[TM]. \tag{4}$$

This equation predicts that τ_{PL}-[TM] relation shows a straight line under low [TM^{3+}] excitation conditions for high [TM] regime. By fitting the data in Fig. 3 using Eq. (4) with a reported intrinsic τ_R value of 20 ns at 300 K for the FX_A peak[15] and $m^*_{ex} = 0.242m_0$,[36] where m_0 is a free electron mass, we obtain $\sigma_{ex} = 2.4 \times 10^{-15}$ cm^2. This value is close to the electron capture-cross-section (σ_n) of several trap levels in ZnO[37] and σ_n of $Fe^{3+/2+}$ center in GaN (1.9×10^{-15} cm^2),[38] and is not far from σ_n of EL2 in GaAs (4.7×10^{-16} cm^2).[39] We note that the data point of N6 deviates from the fitted line in Fig. 3. One of likely reasons for this deviation is that the concentration ratio between Al and TM of N6 is much higher than other samples, resulting in reduced probability of nonradiative recombination.

In Fig. 4, room-temperature R_q of the FX_A peak in TM-doped ZnO epilayers are plotted as a function of τ_{PL} using diamond legends. Solid line shows the ideal $\eta_{int} - \tau_{PL}$ line drawn using the relationship derived from Eqs. (1) and (2); i.e., $\eta_{int} = \tau_{PL}/\tau_R$, assuming the intrinsic τ_R of 20 ns.[15] For comparison, $R_q - \tau_{PL}$ relationships reported for UID-ZnO epilayers grown by laser-assisted molecular-beam epitaxy (L-MBE),[15] plasma-assisted molecular-beam epitaxy (PA-MBE),[21] and metalorganic chemical vapor deposition (MOCVD)[22,23] are plotted. In these epilayers,[15,21–23] major NRCs are the "native" one, $V_{Zn}X$.[14,15] It is obvious that the plots of TM-doped and UID ZnO lie on the same line. As τ_{PL} (=τ_{NR}) of the UID-ZnO in Refs. 15 and 21–23 are one to two orders of magnitude longer than our TM-doped ZnO, [$V_{Zn}X$] in those UID-ZnO are estimated to be "lower than" $10^{16} - 10^{17}$ cm^{-3}, because σ_{ex} of native-NRCs ($V_{Zn}X$ complexes) is most likely larger than that of isolated TMs on Ga site. Evidence to support the absolute values of [$V_{Zn}X$] predicted in this study is that *S* of the best O-polar ZnO epilayer[15] has been reaching *S* of a ZnO with [V_{Zn}] under the detection limit (S_{free}), namely, down to 10^{15} cm^{-3}.[15] Consistent with our results, [V_{Zn}] in ZnO and $Mn_{0.015}Zn_{0.985}O$ crystals grown by CVT have been reported to be about 2×10^{16} cm^{-3}.[40]

In summary, room-temperature τ_{PL} of the NBE emission, which approximates $\tau_{minority}$, of nearly TD-free ZnO epilayers was controlled by doping 3*d* TMs having the CTLs within the bandgap. The carrier trapping dynamics due to $Ni^{2+/3+}$ and $Mn^{2+/3+}$ in ZnO were studied using TRPL and PAS measurements. From the linear dependence of τ_{PL} on [TM] for sufficiently TM-doped ZnO, σ_{ex} of isolated TMs was estimated to be 2.4×10^{-15} cm^2. Because σ_{ex} of native-NRCs composed of $V_{Zn}X$ complexes is most likely larger than this value, the proportionality relationship between η_{int} and τ_{PL} observed universally in UID and TM-doped ZnO and Eq. (3) lead to the conclusion that [$V_{Zn}X$] in the state-of-the-art, nearly TD-free, UID-ZnO epitaxial films grown by L-MBE, PA-MBE, and

MOCVD are lower than $1 \times 10^{16}\,\mathrm{cm}^{-3}$. Such low [NRC] is most likely achieved by precise controllability of the surface stoichiometry keeping the step-flow growth mode at high T_g.

The authors would like to thank T. Ohtomo and H. Nakasawa for help with the experiments and data analyses. This study was supported in part by Management Expenses Grants for National Universities Corporations, MEXT, Japan.

[1]For example, see http://iopscience.iop.org/0268-1242/20/4, "Special issue: Oxide semiconductors," *Semicond. Sci. Technol.* edited by M. Kawasaki and T. Makino, 2015, Vol. 20, Issue 4.
[2]A. Tsukazaki, A. Ohtomo, T. Onuma, M. Ohtani, T. Makino, M. Sumiya, K. Ohtani, S. F. Chichibu, S. Fuke, Y. Segawa, H. Ohno, H. Koinuma, and M. Kawasaki, Nat. Mater. **4**, 42 (2005).
[3]A. Tsukazaki, M. Kubota, A. Ohtomo, T. Onuma, K. Ohtani, H. Ohno, S. F. Chichibu, and M. Kawasaki, Jpn. J. Appl. Phys., Part 2 **44**, L643 (2005).
[4]K. Nakahara, S. Akasaka, H. Yuji, K. Tamura, T. Fujii, Y. Nishimoto, D. Takamizu, A. Sasaki, T. Tanabe, H. Takasu, H. Amaike, T. Onuma, S. F. Chichibu, A. Tsukazaki, A. Ohtomo, and M. Kawasaki, Appl. Phys. Lett. **97**, 013501 (2010).
[5]D. Reynolds, D. Look, B. Jogai, and H. Morkoc, Solid State Commun. **101**, 643 (1997).
[6]D. G. Thomas, J. Phys. Chem. Solids **15**, 86 (1960).
[7]S. Nakamura and G. Fasol, *The Blue Laser Diode* (Springer, Berlin, 1997).
[8]S. Nakamura, M. Senoh, N. Iwasa, and S.-I. Nagahama, Jpn. J. Appl. Phys., Part 2 **34**, L797 (1995).
[9]"Efficient blue light-emitting diodes leading to bright and energy-saving white light sources," in the statement of Scientific Background on the Nobel Prize in Physics 2014, compiled by the Class for Physics of the Royal Swedish Academy of Sciences, 7 October 2014.
[10]E. Oshima, H. Ogino, I. Niikura, K. Maeda, M. Sato, M. Ito, and T. Fukuda, J. Cryst. Growth **260**, 166 (2004).
[11]P. F. Carcia, R. S. McLean, M. H. Reilly, and G. Nunes, Jr., Appl. Phys. Lett. **82**, 1117 (2003); S. Masuda, K. Kitamura, Y. Okumura, S. Miyatake, H. Tabata, and T. Kawai, J. Appl. Phys. **93**, 1624 (2003).
[12]S. Sasa, T. Hayafuji, M. Kawasaki, K. Koike, M. Yano, and M. Inoue, Jpn. J. Appl. Phys., Part 1 **47**, 2845 (2008); A. Tsukazaki, H. Yuji, S. Akasaka, K. Tamura, K. Nakahara, T. Tanabe, H. Takasu, A. Ohtomo, and M. Kawasaki, Appl. Phys. Express **1**, 055004 (2008).
[13]A. Tsukazaki, A. Ohtomo, T. Kita, Y. Ohno, H. Ohno, and M. Kawasaki, Science **315**, 1388 (2007); A. Tsukazaki, S. Akasaka, K. Nakahara, Y. Ohno, H. Ohno, D. Maryenko, A. Ohtomo, and M. Kawasaki, Nat. Mater. **9**, 889 (2010).
[14]S. F. Chichibu, A. Uedono, A. Tsukazaki, T. Onuma, M. Zamfirescu, A. Ohtomo, A. Kavokin, G. Cantwell, C. W. Litton, T. Sota, and M. Kawasaki, Semicond. Sci. Technol. **20**, S67 (2005).
[15]S. F. Chichibu, T. Onuma, M. Kubota, A. Uedono, T. Sota, A. Tsukazaki, A. Ohtomo, and M. Kawasaki, J. Appl. Phys. **99**, 093505 (2006).
[16]S. F. Chichibu, A. Uedono, T. Onuma, T. Sota, B. A. Haskell, S. P. DenBaars, J. S. Speck, and S. Nakamura, Appl. Phys. Lett. **86**, 021914 (2005); S. F. Chichibu, K. Hazu, Y. Ishikawa, M. Tashiro, H. Namita, S. Nagao, K. Fujito, and A. Uedono, J. Appl. Phys. **111**, 103518 (2012).
[17]M. A. Gluba and N. H. Nickel, Phys. Rev. B **87**, 085204 (2013).
[18]M. G. Wardle, J. P. Goss, and P. R. Briddon, Phys. Rev. B **72**, 155108 (2005).
[19]E. Malguth, A. Hoffmann, and M. R. Phillips, Phys. Status Solidi B **245**, 455 (2008).
[20]S. J. Pearton, D. P. Norton, M. P. Ivill, A. F. Hebard, J. M. Zavada, W. M. Chen, and I. A. Buyanova, IEEE Trans. Electron Devices **54**, 1040 (2007).
[21]D. Takamizu, Y. Nishimoto, S. Akasaka, H. Yuji, K. Tamura, K. Nakahara, T. Onuma, T. Tanabe, H. Takasu, M. Kawasaki, and S. F. Chichibu, J. Appl. Phys. **103**, 063502 (2008).
[22]E. Fujimoto, M. Sumiya, T. Ohnishi, K. Watanabe, M. Lippmaa, Y. Matsumoto, and H. Koinuma, Appl. Phys. Express **2**, 045502 (2009).
[23]E. Fujimoto, K. Watanabe, Y. Matsumoto, H. Koinuma, and M. Sumiya, Appl. Phys. Lett. **97**, 131913 (2010).
[24]K. Furusawa, H. Nakasawa, Y. Ishikawa, and S. F. Chichibu, Jpn. J. Appl. Phys., Part 1 **53**, 100301 (2014).
[25]S. F. Chichibu, T. Yoshida, T. Onuma, and H. Nakanishi, J. Appl. Phys. **91**, 874 (2002).
[26]Y. Sawai, K. Hazu, and S. F. Chichibu, J. Appl. Phys. **108**, 063541 (2010).
[27]Optical properties of the bulk ZnO single crystal with the same purity as the polycrystalline target have been given in S. F. Chichibu, T. Sota, G. Cantwell, D. B. Eason, and C. W. Litton, J. Appl. Phys. **93**, 756–758 (2003).
[28]S. Akasaka, K. Nakahara, H. Yuji, A. Tsukazaki, A. Ohtomo, and M. Kawasaki, Appl. Phys. Express **4**, 035701 (2011).
[29]B. K. Meyer, H. Alves, D. M. Hoffmann, W. Kriegseis, D. Foster, F. Bertram, J. Christen, A. Hoffmann, M. Straßbrug, M. Dworzak, U. Haboeck, and A. V. Rodina, Phys. Status Solidi B **241**, 231 (2004).
[30]B. K. Meyer, J. Sann, D. M. Hoffman, and A. Zeuner, Semicond. Sci. Technol. **20**, S62 (2005).
[31]R. Krause-Rehberg and H. S. Leipner, *Positron Annihilation in Semiconductors*, Solid-State Sciences Vol. 127 (Springer, Berlin, 1999); P. G. Coleman, *Positron Beams and Their Application* (World Scientific, Singapore, 2000).
[32]A. Uedono, T. Koida, A. Tsukazaki, M. Kawasaki, Z. Q. Chen, S. F. Chichibu, and H. Koinuma, J. Appl. Phys. **93**, 2481 (2003).
[33]T. Ghoshal, S. Kar, S. Biswas, S. K. De, and P. M. G. Nambissan, J. Phys. Chem. C **113**, 3419 (2009).
[34]H. J. Zhang, Z. Q. Chen, S. J. Wang, A. Kawasuso, and N. Morishita, Phys. Rev. B **82**, 035439 (2010).
[35]D. C. Reynolds, D. C. Look, and B. Jogai, J. Appl. Phys. **89**, 6189 (2001).
[36]C. Klingshirn, Phys. Status Solidi B **244**, 3027 (2007).
[37]F. D. Auret, S. A. Goodman, M. J. Legodi, W. E. Meyer, and D. C. Look, Appl. Phys. Lett. **80**, 1340 (2002).
[38]T. Aggerstam, A. Pinos, S. Marcinkevicius, M. Linnarsson, and S. Lourdudodd, J. Electron. Mater. **36**, 1621 (2007).
[39]A. Mitonneau, A. Mircea, G. M. Martin, and D. Pons, Rev. Phys. Appl. (France) **14**, 853 (1979).
[40]F. Tuomisto, A. Mycielski, and K. Grasza, Superlattices Microstruct. **42**, 218 (2007).